

## Electronic Supplementary Information (ESI)

### Structure and Magnetic Exchange in Hetero-metallic 3d-3d transition metal triethanolamine clusters

Stuart K. Langley,<sup>a</sup> Nicholas F. Chilton,<sup>a</sup> Boujemaa Moubaraki<sup>a</sup> and Keith S. Murray<sup>\*, a</sup>

<sup>a</sup> School of Chemistry, Monash University, Clayton, Victoria 3800, Australia

pp. 2 – 5 **Tables S1 to S14**; Selected bond lengths and bond-valence sum calculations for compounds **1** to **7**.

pp. 6 – 12 **Figures S1 to S14**; Plots of DC susceptibilities, exchange coupling schemes and Zeeman energy levels for **4** and **5**, then for **2**, **3**, **6** and **7**.

pp. 13 – 16 **Figures S15 to S21**; Plots of AC in-phase and out-of phase susceptibilities for complexes **2**, **3**, **6** and **7**.

pp. 16 - 19 **Figures S22 to S27**; Crystal packing diagrams for **2**, **3**, **5**, **6** and **7**.

Mn1-O3	1.886(5)	Mn2-O2	1.896(5)	Co3-O9	1.883(5)	Co1-O9	1.993(5)
Mn1-O3'	1.901(5)	Mn2-O8	1.902(5)	Co3-O5	1.902(5)	Co1-O8	2.001(6)
Mn1-O7'	1.941(5)	Mn2-O3	1.919(5)	Co3-O7	1.902(5)	Co1-O11	2.030(7)
Mn1-O1	1.959(5)	Mn2-O6	1.947(5)	Co3-O6	1.916(5)	Co1-O12	2.065(6)
Mn1-O2	2.156(5)	Mn2-O4	2.149(6)	Co3-N2	1.943(7)	Co1-N3	2.238(7)
Mn1-O5'	2.343(5)	Mn2-O5	2.240(5)	Co3-N1	1.968(7)		

**Table S1.** Selected bond lengths for **1**. Symmetry transformation: (') - x, - y, 1 - z.

Atoms	Mn(II)	Mn(III)	Mn(IV)	Co(II)	Co(III)
Mn1	3.40	<b>3.13</b>	3.07	2.56	2.24
Mn2	3.53	<b>3.26</b>	3.19	2.66	2.33
Co3	4.46	4.23	4.18	3.10	<b>3.11</b>
Co1	2.49	2.32	2.28	<b>1.83</b>	1.76

**Table S2.** Bond valence sum calculations for **1**. The oxidation state for each metal is the whole number closest to the value in bold.

It is clear that Mn1 and Mn2 are Mn<sup>III</sup> ions due to the presence of Jahn-Teller distorted octahedral geometries, with the BVS calculations backing this up. The remaining ions are initially assigned as Co<sup>II</sup> and Co<sup>III</sup> over Mn<sup>II</sup> and Mn<sup>IV</sup> respectively due to the better correlation with the BVS parameter. It is however difficult to say for certain, just from looking at the x-ray data. Charge balance considerations and microanalysis then backs up the BVS analysis.

Mn1-O5	2.176(3)	Mn1-O1'	2.402(3)	Mn2-O6	1.955(3)	Co1-O11	1.897(3)
Mn1-O4	2.201(3)	Mn1-N1	2.431(3)	Mn2-O9	2.146(3)	Co1-O10	1.908(2)
Mn1-O2	2.239(3)	Mn2-O4'	1.892(3)	Mn2-O3	2.284(3)	Co1-O3	1.909(3)
Mn1-O3	2.242(3)	Mn2-O8	1.910(2)	Co1-O5	1.874(2)	Co1-N2	1.984(3)
Mn1-O1	2.262(3)	Mn2-O1'	1.918(2)	Co1-O6	1.885(3)		

**Table S3.** Selected bond lengths for **2**. Symmetry transformation: (') - x, 1 - y, - z.

Atoms	Mn(II)	Mn(III)	Mn(IV)	Co(II)	Co(III)
Mn1	<b>1.96</b>	1.79	1.77	1.43	1.31
Mn2	3.47	<b>3.20</b>	3.14	2.61	2.29
Co1	4.46	4.17	4.10	2.89	<b>3.02</b>

**Table S4.** Bond valence sum calculations for **2**. The oxidation state for each metal is the whole number closest to the value in bold.

BVS calculations deliver no ambiguity here. Microanalysis and charge balance considerations again confirm the type of ion and its oxidation state.

Mn1-O10	1.881(4)	Mn1-O5	2.243(4)	Ni1-N1	2.125(5)	Ni2-O5	2.066(4)
Mn1-O4	1.889(4)	Ni1-O7'	2.025(5)	Ni1-O1'	2.153(4)	Ni2-O11	2.074(5)
Mn1-O8	1.954(4)	Ni1-O4	2.028(4)	Ni2-O12	2.029(5)	Ni2-N2	2.106(6)
Mn1-O1'	1.984(4)	Ni1-O2	2.093(4)	Ni2-O9	2.043(4)		
Mn1-O6	2.149(5)	Ni1-O1	2.123(5)	Ni2-O10	2.054(4)		

**Table S5.** selected bond lengths for **3**. Symmetry transformation: (') 1 - x, 1 - y, 1 - z.

Atoms	Mn(II)	Mn(III)	Mn(IV)	Ni(II)
Mn1	3.49	<b>3.25</b>	3.20	2.48
Ni1	2.74	2.56	2.52	<b>1.91</b>
Ni2	2.95	2.76	2.66	<b>2.08</b>

**Table S6.** Bond valence sum calculations for **3**. The oxidation state for each metal is the whole number closest to the value in bold.

Jahn-Teller distortions from the bond length data and the BVS calculation suggest Mn1 is a Mn<sup>III</sup> ion. BVS calculations then suggest the remaining ions are Ni<sup>II</sup>. This is backed up from previous knowledge for a analogous {Mn<sup>II</sup><sub>4</sub>Mn<sup>III</sup><sub>2</sub>} cluster, were the Ni1 site in **3** is a Mn<sup>II</sup> ion and is seven coordinate. With the inclusion the Ni<sup>II</sup> ion - Ni1 is now six coordinate. Comparing the bond length data with the {Mn<sup>II</sup><sub>4</sub>Mn<sup>III</sup><sub>2</sub>} cluster the Ni<sup>II</sup> site - Ni2 now has much shorter bond lengths than in the Mn cluster, as expected if a Ni<sup>II</sup> ion is now present.

Mn2-O7	1.8533(10)	Mn2-O3'	1.9729(10)	Co1-O4	2.0039(10)	Co1-O3	2.0873(10)
Mn2-O4	1.8816(10)	Mn2-O6	2.2523(11)	Co1-O2	2.0332(10)	Co1-N1	2.1563(11)
Mn2-O8	1.8929(10)	Mn2-O1'	2.3244(11)	Co1-O1	2.0381(10)	Co1-O3'	2.2846(10)

**Table S7.** Selected bond lengths for **4**. Symmetry transformation: (') 1 - x, 2 - y, - z.

Atoms	Mn(II)	Mn(III)	Mn(IV)	Co(II)	Co(III)
Mn2	3.51	<b>3.23</b>	3.17	2.64	2.32
Co1	2.67	2.46	2.42	<b>2.01</b>	1.76

**Table S8.** Bond valence sum calculations for **4**.

The presence of Jahn-Teller distortions confirm the Mn<sup>III</sup> assignment. The Co<sup>II</sup> site is then supported by the BVS calculation and microanalysis.

Mn1-O2	2.1177(17)	Mn1-N2'	2.282(2)	Fe1-O4	1.9493(18)	Fe1-O7	2.1328(17)
Mn1-O3	2.1758(17)	Mn1-N1	2.410(2)	Fe1-O6	1.9706(18)		
Mn1-O1	2.251(2)	Mn1-O1'	2.534(2)	Fe1-O3'	1.9838(17)		
Mn1-O7'	2.2554(17)	Fe1-O2	1.9318(19)	Fe1-O5	2.053(2)		

**Table S9.** Selected bond lengths for **5**. Symmetry transformation: (') - x, - y, - z.

Atoms	Mn(II)	Mn(III)	Mn(IV)	Fe(II)	Fe(III)
Mn1	<b>1.84</b>	1.74	1.71	1.46	1.68
Fe1	3.42	3.15	3.09	2.94	<b>3.14</b>

**Table S10.** Bond valence sum calculations for **5**. The oxidation state for each metal is the whole number closest to the value in bold.

The seven coordinate divalent ion is assigned as Mn<sup>II</sup>, with the trivalent ion assigned as Fe<sup>III</sup> due to the absence of octahedral axial distortions. BVS calculations and microanalysis confirm this assignment.

Mn1-O12	2.128(5)	Mn2-F7	1.863(4)	Mn3-O13	1.963(5)	Co1-N3	1.986(6)
Mn1-O1	2.134(5)	Mn2-O14	1.946(5)	Mn3-O9	2.138(5)	Co2-O13	1.880(5)
Mn1-O10	2.183(5)	Mn2-O2	1.954(5)	Mn3-O6	2.246(5)	Co2-O12	1.880(5)
Mn1-O5	2.299(5)	Mn2-O8	2.221(5)	Co1-O1	1.881(5)	Co2-O6	1.923(5)
Mn1-O4	2.332(5)	Mn2-O4	2.272(5)	Co1-O2	1.882(5)	Co2-N7	1.944(7)
Mn1-N4	2.344(6)	Mn3-O10	1.839(5)	Co1-O4	1.927(5)	Co2-N8	1.951(7)
Mn1-O6	2.376(5)	Mn3-F11	1.853(4)	Co1-N1	1.949(6)	Co2-N6	1.955(6)
Mn2-O10	1.830(5)	Mn3-O14	1.959(5)	Co1-N2	1.954(6)		

**Table S11.** Selected bond lengths for **6**.

Atoms	Mn(II)	Mn(III)	Mn(IV)	Co(II)	Co(III)
Mn1	<b>2.09</b>	1.95	1.91	1.53	1.36
Mn2	3.42	<b>3.14</b>	3.05	2.64	2.36
Mn3	3.48	<b>3.19</b>	3.10	2.68	2.38
Co1	4.46	4.23	<b>4.07</b>	2.98	<b>3.15</b>
Co2	4.55	4.31	<b>4.16</b>	3.03	<b>3.24</b>

**Table S12.** Bond valence sum calculations for **6**. The oxidation state for each metal is the whole number closest to the value in bold.

The seven coordinate site is assigned as Mn<sup>II</sup>, with the two Mn<sup>III</sup> ions displaying Jahn-Teller distorted octahedral geometries. The BVS calculation is ambiguous in this case, but due to charge balance considerations the ions must be 3+. With no Jahn-Teller distortion and with the microanalysis data the ions were confirmed as Co<sup>III</sup>.

Mn1-O9	2.094(3)	Mn2-O4	1.906(3)	Mn3-O19	2.269(2)	Co1-O19	1.929(3)
Mn1-O4	2.164(2)	Mn2-O2	1.929(2)	Mn3-O4	2.292(2)	Co1-N2	1.988(3)
Mn1-O2	2.188(3)	Mn2-O7	1.954(2)	Mn3-O14	2.333(3)	Co2-O18	1.863(3)
Mn1-O1	2.288(3)	Mn2-O5	2.138(3)	Mn3-N3	2.390(3)	Co2-O7	1.872(2)
Mn1-O3	2.291(3)	Mn2-O8	2.270(2)	Co1-O10	1.863(2)	Co2-O16	1.901(3)
Mn1-O19	2.347(2)	Mn3-O10	2.096(3)	Co1-O9	1.868(2)	Co2-O15	1.904(2)
Mn1-N1	2.421(3)	Mn3-O18	2.161(2)	Co1-O11	1.912(2)	Co2-O8	1.915(2)
Mn2-O6	1.896(3)	Mn3-O8	2.251(3)	Co1-O13	1.912(2)	Co2-N4	1.986(3)

**Table S13.** Selected bond lengths for **7**.

Atoms	Mn(II)	Mn(III)	Mn(IV)	Co(II)	Co(III)
Mn1	<b>2.09</b>	1.95	1.91	1.54	1.41
Mn2	3.47	<b>3.20</b>	3.14	2.61	2.29
Mn3	<b>2.08</b>	1.94	1.90	1.53	1.40
Co1	4.44	4.13	<b>4.04</b>	3.22	<b>3.01</b>
Co2	4.50	4.18	<b>4.08</b>	3.27	<b>3.04</b>

**Table S14.** Bond valence sum calculations for **7**. The oxidation state for each metal is the whole number closest to the value in bold.

The two seven-coordinate sites are assigned as Mn<sup>II</sup>, with the Mn<sup>III</sup> ion displaying a Jahn-Teller distorted octahedral geometry. Again the BVS calculation is ambiguous, but again due to charge balance considerations the ions must be 3+. With no Jahn-Teller distortion and with the microanalysis data the ions were confirmed as Co<sup>III</sup>.

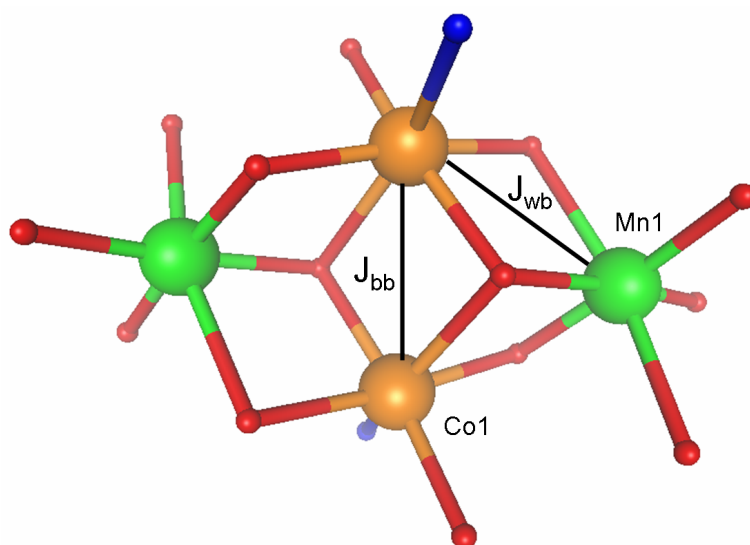


**Fig. S1** Exchange coupling scheme for **4**. Mn<sup>III</sup> green; Co<sup>II</sup> brown.

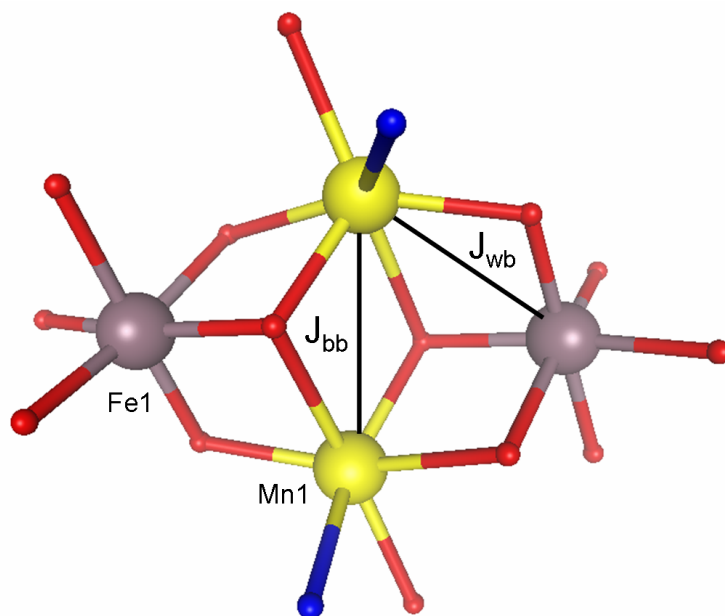


**Fig. S2** Exchange coupling scheme for **5**. Fe<sup>III</sup> grey; Mn<sup>II</sup> yellow. Note that  $J_{wb} = J_1$  in the script and  $J_{bb}$

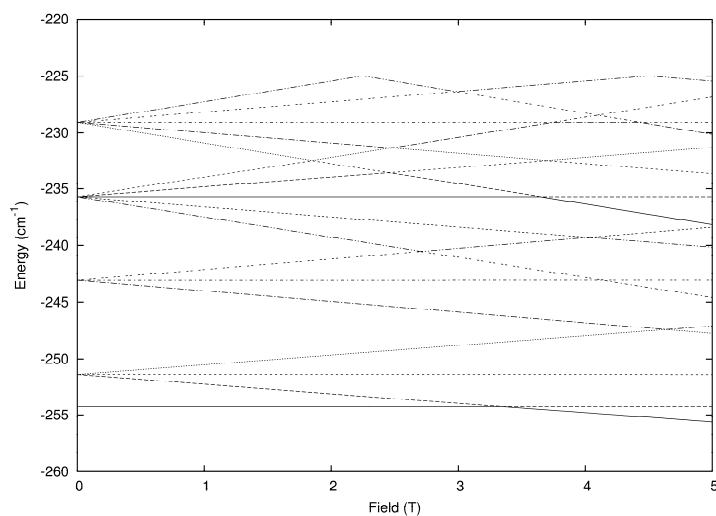


**Fig. S3** Plot of low-lying Zeeman energy levels for  $[\text{Mn}^{\text{II}}_2\text{Fe}^{\text{III}}_2(\text{teaH})_2(\text{paa})_4](\text{NO}_3)_2 \cdot 2\text{MeOH} \cdot \text{CH}_2\text{Cl}_2$  **5**, using the parameters for best-fit given in the text. Note in zero-field the  $S$  (ground) is 0 with  $S = 1$  above. The  $M_s = 0$  crosses with  $M_s = -1$  at  $\sim 3.2$  Tesla.

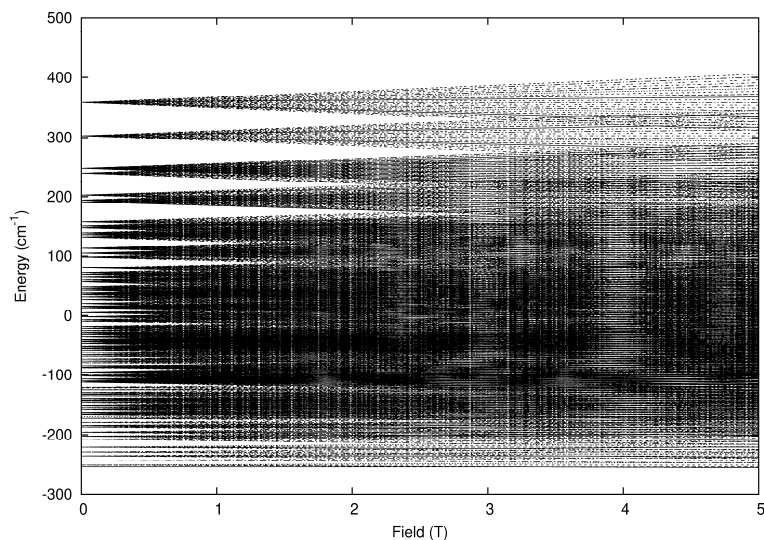


**Fig. S4** Continuum-like full Zeeman energy levels diagram for  $[\text{Mn}^{\text{II}}_2\text{Fe}^{\text{III}}_2(\text{teaH})_2(\text{paa})_4](\text{NO}_3)_2 \cdot 2\text{MeOH} \cdot \text{CH}_2\text{Cl}_2$  **5**, calculated using the best-fit parameters.

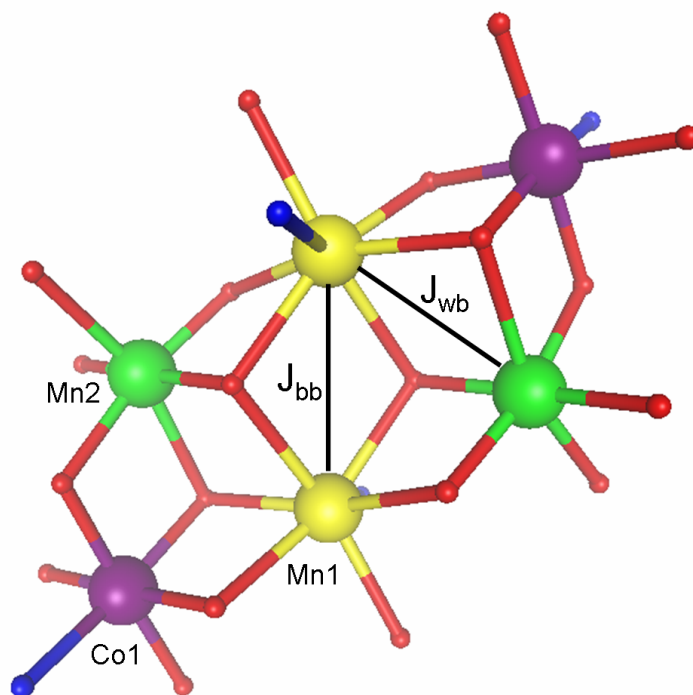


**Fig. S5** Exchange coupling scheme for **2**. Mn<sup>III</sup> green; Mn<sup>II</sup> yellow.

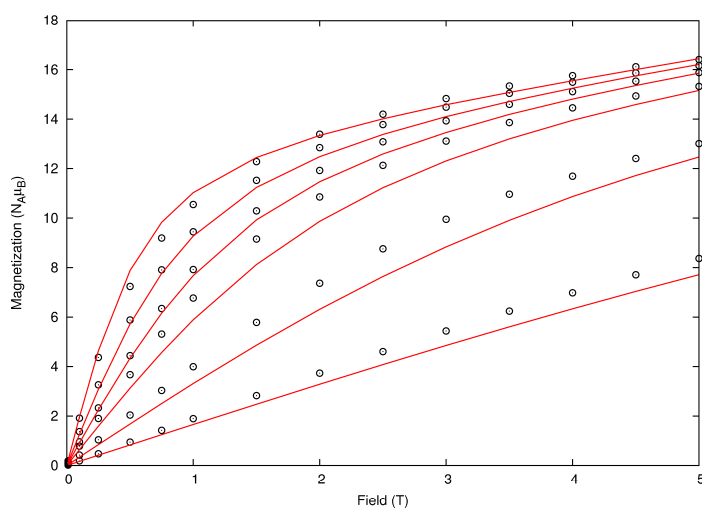


**Fig. S6.** Plot of  $M$  vs.  $H$  at temperatures - 2 (top), 3, 4, 5.5, 10 and 20 K (bottom) for **2**. Solid red lines are calculated using the parameters of Fit 2 in the text.

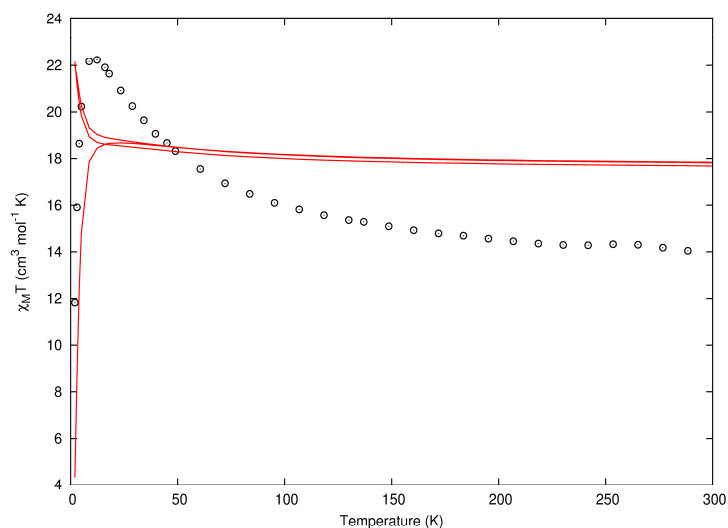


**Fig. S7** Plot of  $\chi_M T$ , per mol., vs. temperature (open circles) for  $[\text{Mn}^{\text{II}}_2\text{Mn}^{\text{III}}_2\text{Co}^{\text{III}}_2(\text{teaH})_4(\text{OMe})_2(\text{acac})_4](\text{NO}_3)_2 \cdot 2\text{MeOH}$  (**2**). The lower red line is that calculated using the Fit 2 set of parameters given in the text and a DC field of 1 T. The higher red lines, below 10 K, are for fields of 0.1 and 0.01 T.

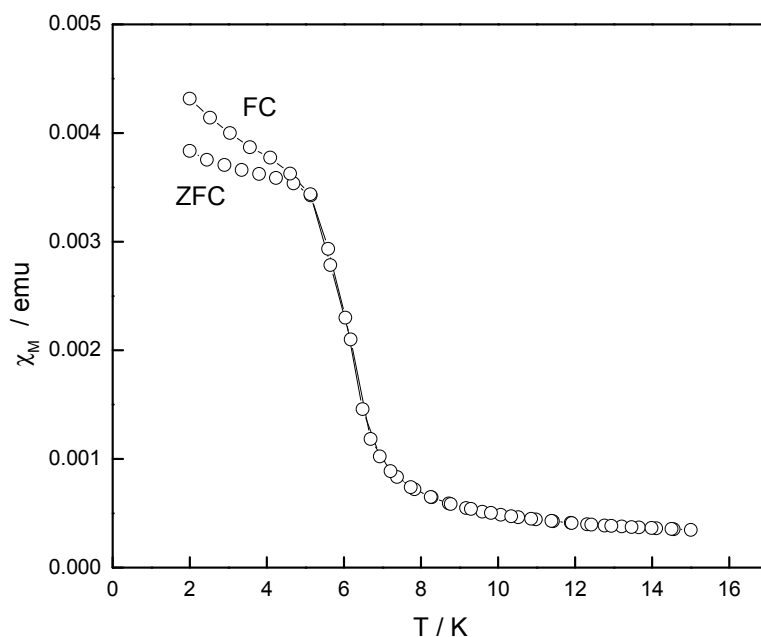


**Fig. S8** Plot of FC and ZFC susceptibilities for  $[\text{Mn}^{\text{III}}_2\text{Ni}^{\text{II}}_4(\text{teaH}_2)_2(\text{teaH})_2(\text{O}_2\text{CMe})_8] \cdot 2\text{MeCN}$  (**3**), showing bifurcation at 5 K (lines just join the points).

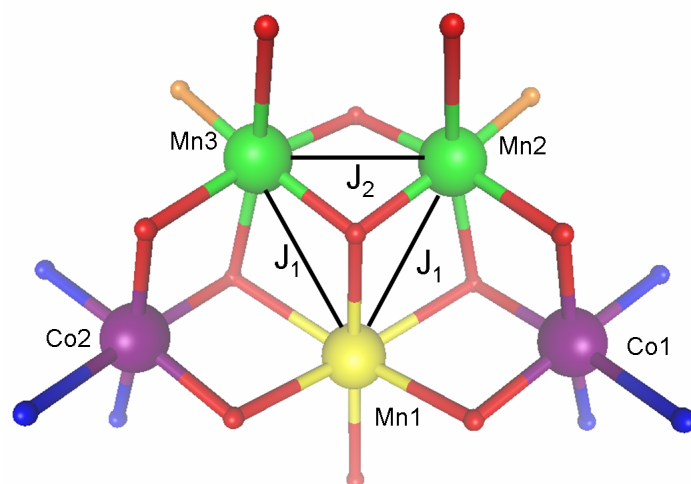


**Fig. S9** Exchange coupling scheme for **6**. Mn<sup>III</sup> green; Mn<sup>II</sup> yellow; Co<sup>III</sup> purple.

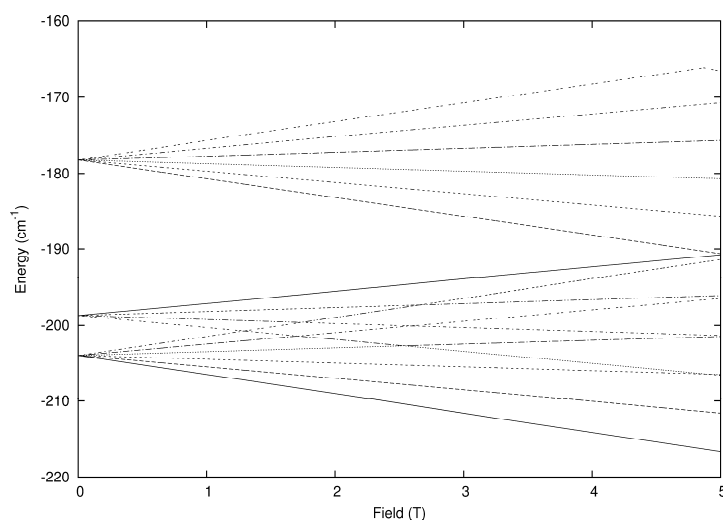


**Fig. S10** Plot of low-lying Zeeman energy levels for  $[\text{Mn}^{\text{II}}\text{Mn}^{\text{III}}_2\text{Co}^{\text{III}}_2(\text{O})(\text{teaH})_2(\text{dea})(\text{Iso})(\text{OMe})(\text{F})_2(\text{Phen})_2](\text{BF}_4)(\text{NO}_3)\cdot 3\text{MeOH}$  **6**, using the parameters for best-fit given in the text. Note in zero-field the  $S$  (ground) is  $5/2$  with  $S = 3/2$  above.

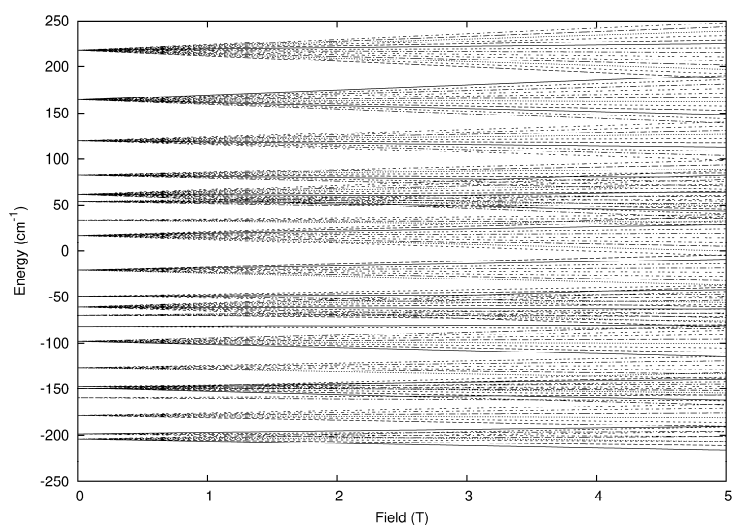


**Fig. S11** Continuum-like full Zeeman energy levels diagram for  $[\text{Mn}^{\text{II}}\text{Mn}^{\text{III}}_2\text{Co}^{\text{III}}_2(\text{O})(\text{teaH})_2(\text{dea})(\text{Iso})(\text{OMe})(\text{F})_2(\text{Phen})_2](\text{BF}_4)(\text{NO}_3)\cdot 3\text{MeOH}$  **6**, calculated using the best-fit parameters given in the text.

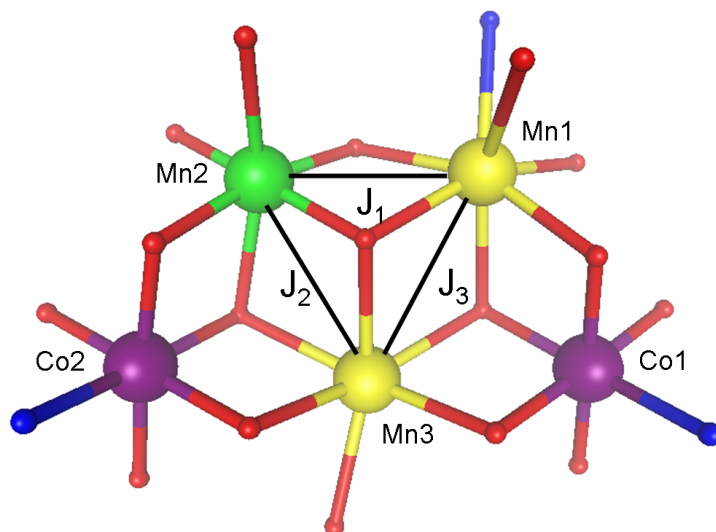


**Fig. S12** Exchange coupling scheme for **7**. Mn<sup>III</sup> green; Mn<sup>II</sup> yellow; Co<sup>III</sup> purple.

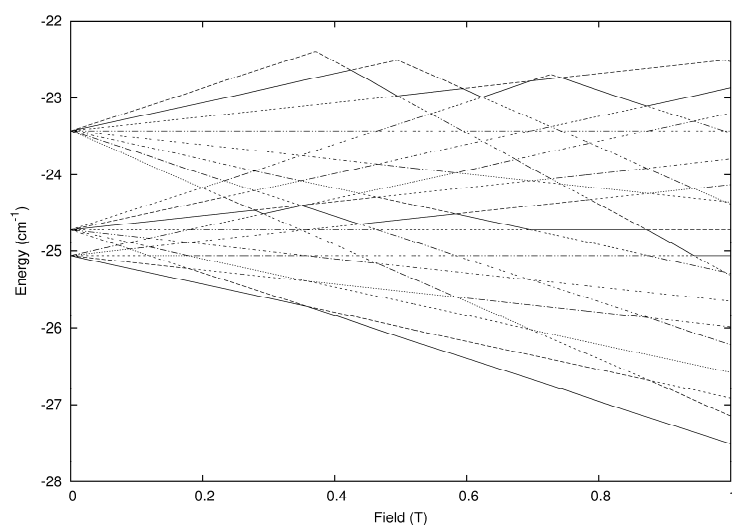


**Fig. S13** Plot of low-lying Zeeman energy levels for  $[\text{Mn}^{\text{II}}_2\text{Mn}^{\text{III}}\text{Co}^{\text{III}}_2(\text{OH})(\text{teaH})_3(\text{teaH}_2)(\text{acac})_3](\text{NO}_3)_2 \cdot 3\text{CH}_2\text{Cl}_2$  (**7**) calculated using the parameters for best-fit given in the text. At zero-field the ground  $S$  is 2 with its lowest  $M_S = -2$  crossing  $M_S$  levels from the next higher  $S$  at  $H \sim 0.39$  T.

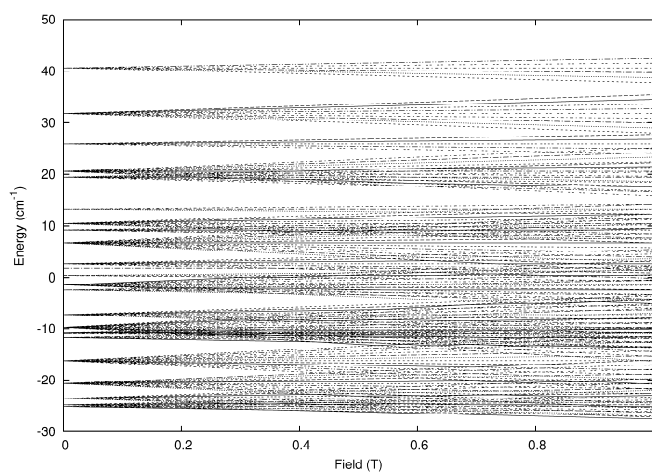


**Fig. S14** Continuum-like full Zeeman energy levels diagram for  $[\text{Mn}^{\text{II}}_2\text{Mn}^{\text{III}}\text{Co}^{\text{III}}_2(\text{OH})(\text{teaH})_3(\text{teaH}_2)(\text{acac})_3](\text{NO}_3)_2 \cdot 3\text{CH}_2\text{Cl}_2$  (**7**), calculated using the best-fit parameters given in the text.

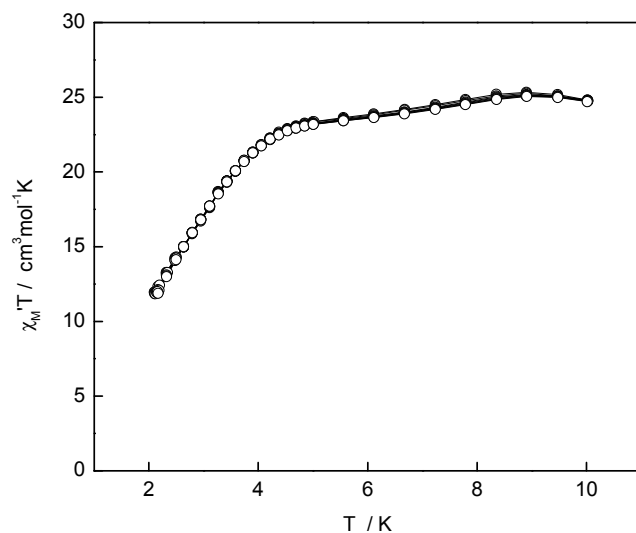


**Fig. S15** Plot of the in-phase AC susceptibility  $\chi_M' T$  vs  $T$  for **2** between 2 and 10 K. The frequencies used were 1500, 1250, 1000, 750, 500, 250, 100 Hz.

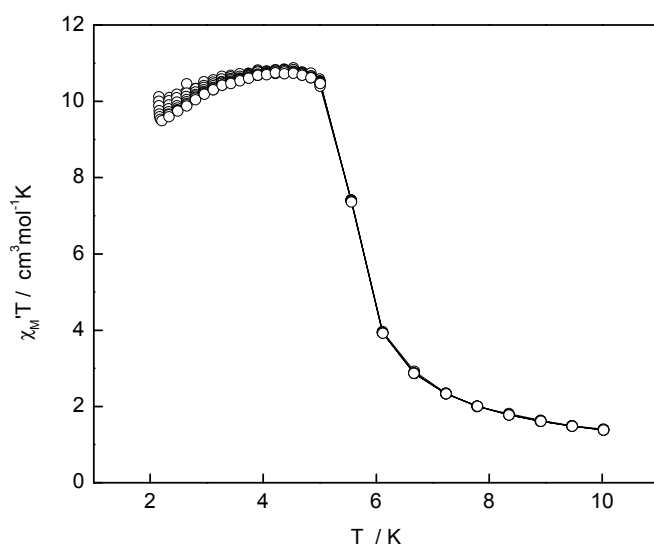


**Fig. S16** Plot of the in-phase AC susceptibility  $\chi_M' T$  vs  $T$  for **3**. The frequencies used were 1500, 1250, 1000, 750, 500, 250, 100 Hz.

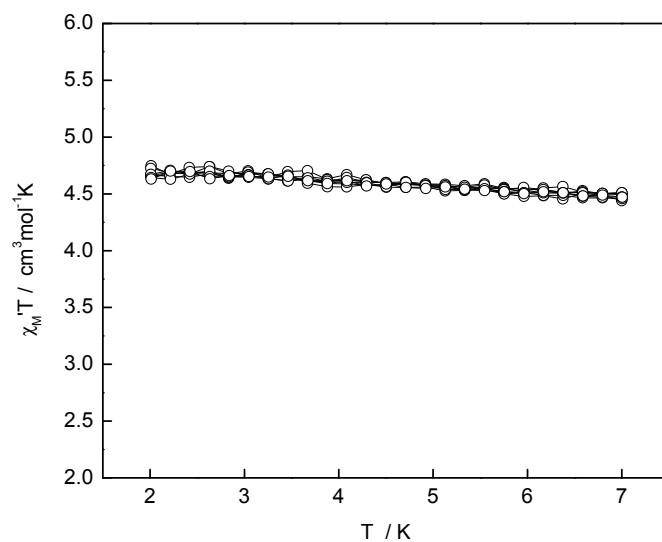


**Fig. S17** Plot of the in-phase AC susceptibility  $\chi_M' T$  vs  $T$  for **6**. The frequencies used were 1500, 1250, 1000, 750, 500, 250 Hz.

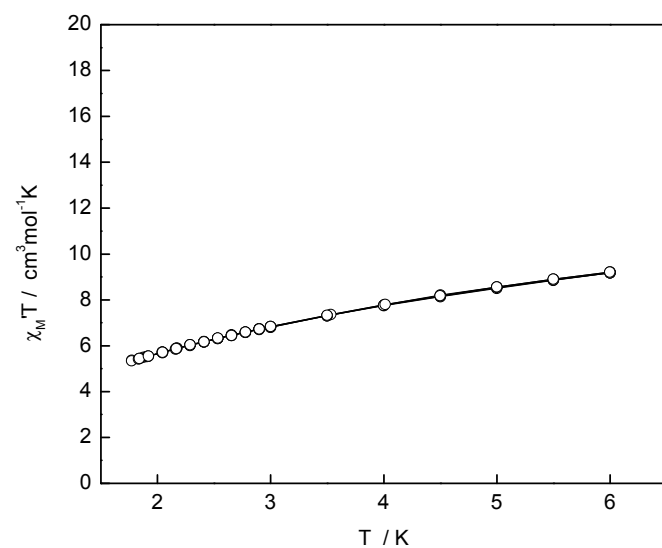


**Fig. S18** Plot of the in-phase AC susceptibility  $\chi_M' T$  vs  $T$  for **7**. The frequencies used were 1500, 1250, 1000, 750, 500 Hz.

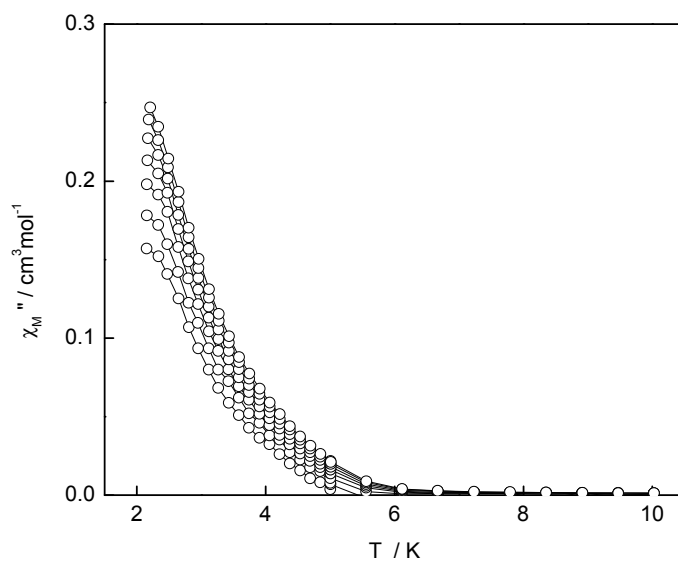


**Fig. S19** Plot of the out-of-phase AC susceptibility  $\chi_M''$  vs  $T$  for **3**. The frequencies used were 1500 (top), 1250, 1000, 750, 500, 250, 100 Hz (bottom).

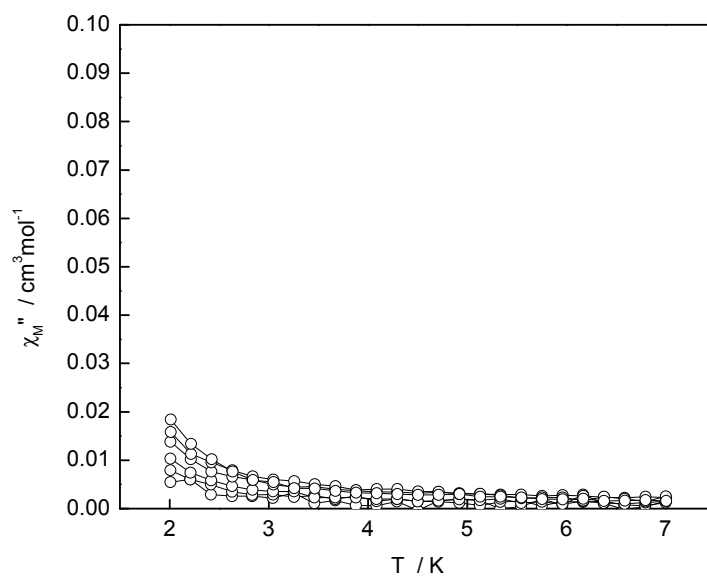


**Fig. S20** Plot of the out-of-phase AC susceptibility  $\chi_M''$  vs  $T$  for **6**. The frequencies used were 1500 (top), 1250, 1000, 750, 500, 250 Hz (bottom).

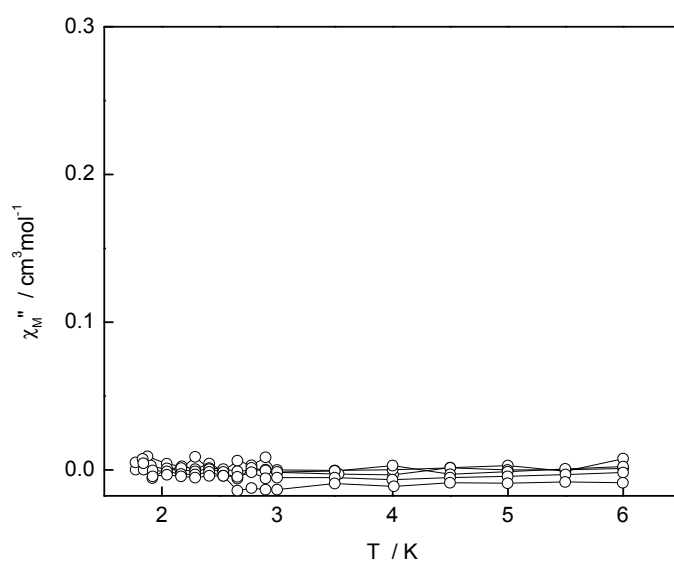


**Fig. S21** Plot of the out-of-phase AC susceptibility  $\chi_M''$  vs  $T$  for **7**. The frequencies used were 1500 (top), 1250, 1000, 750, 500 Hz (bottom).

### Crystal packing diagrams

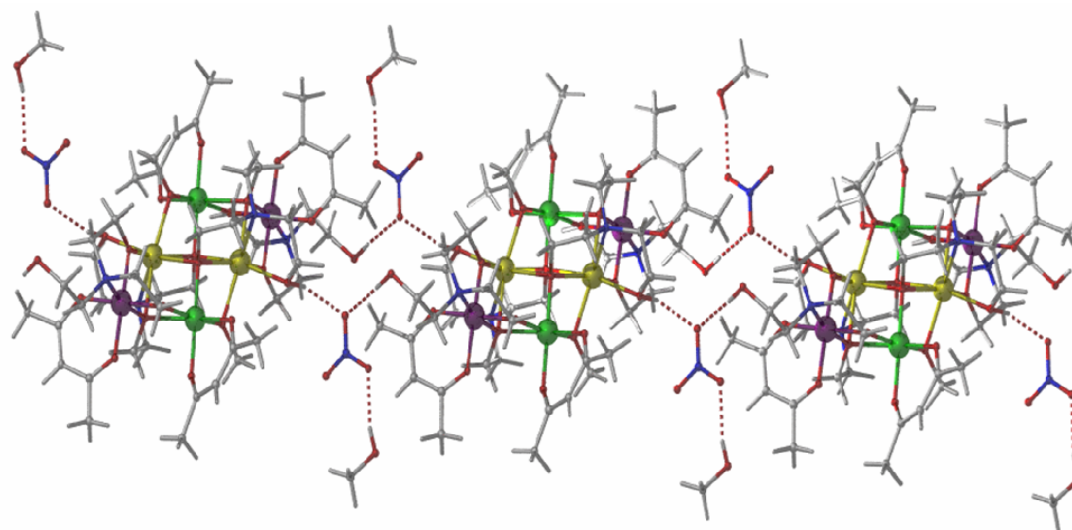


**Fig. S22** Crystal packing for  $[\text{Mn}^{\text{II}}_2\text{Mn}^{\text{III}}_2\text{Co}^{\text{III}}_2(\text{teaH})_4(\text{OMe})_2(\text{acac})_4](\text{NO}_3)_2 \cdot 2\text{MeOH}$  (**2**).

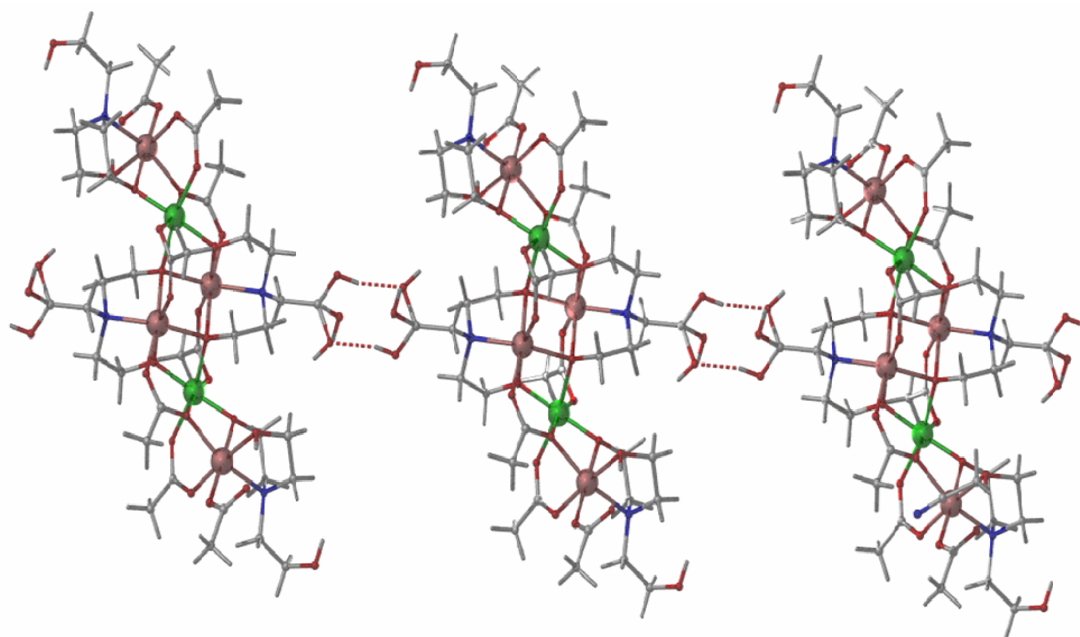


**Fig. S23** Crystal packing for  $[\text{Mn}^{\text{III}}_2\text{Ni}^{\text{II}}_4(\text{teaH}_2)_2(\text{teaH})_2(\text{O}_2\text{CMe})_8]\cdot 2\text{MeCN}$  (**3**)

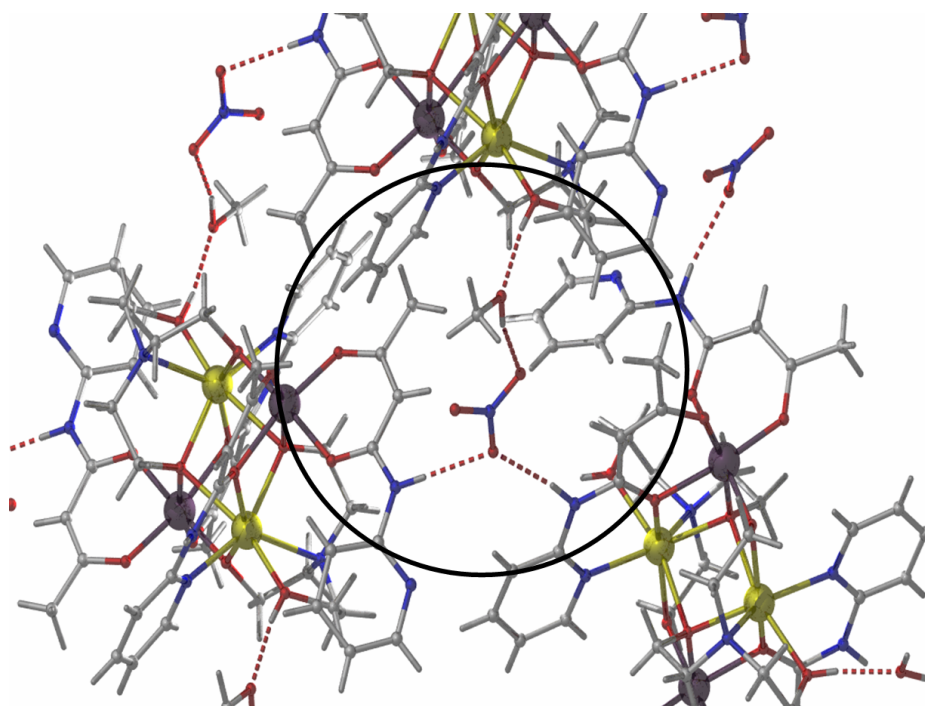


**Fig. S24** Simplified crystal packing for  $[\text{Mn}^{\text{II}}_2\text{Fe}^{\text{III}}_2(\text{teaH})_2(\text{paa})_4](\text{NO}_3)_2\cdot 2\text{MeOH}\cdot \text{CH}_2\text{Cl}_2$  (**5**), showing H-bonding pathways.

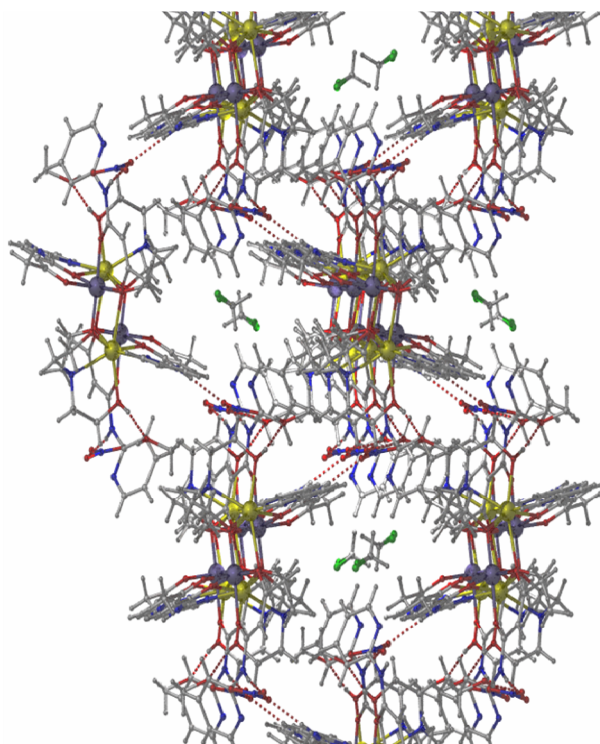


**Fig. S25** Extended crystal packing for  $[\text{Mn}^{\text{II}}_2\text{Fe}^{\text{III}}_2(\text{teaH})_2(\text{paa})_4](\text{NO}_3)_2 \cdot 2\text{MeOH} \cdot \text{CH}_2\text{Cl}_2$  (**5**).

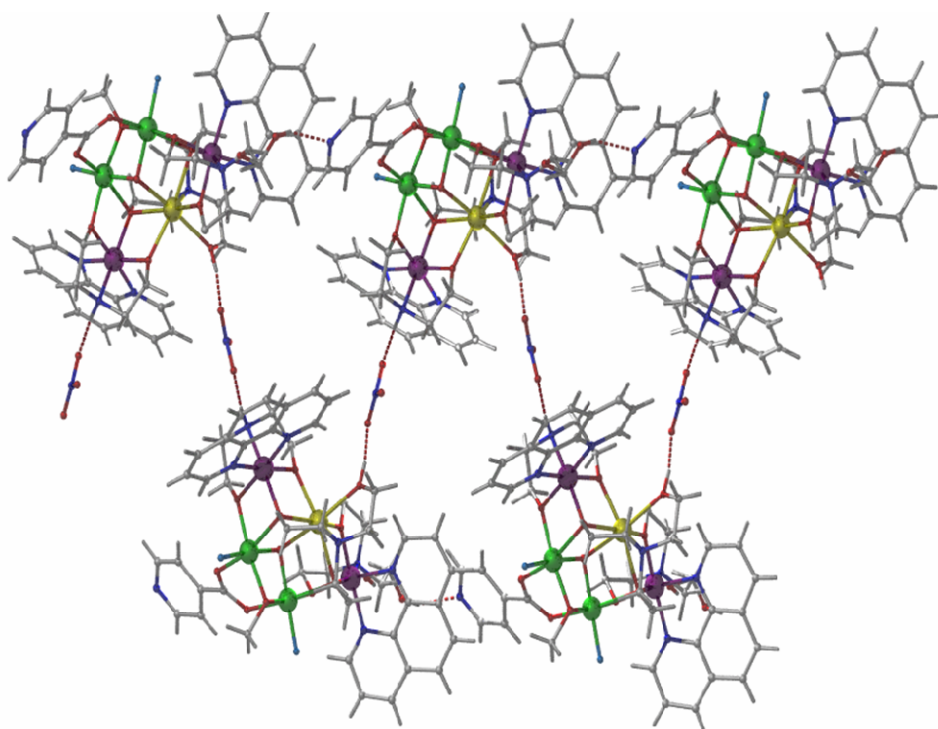


**Fig. S26** Crystal packing for  $[\text{Mn}^{\text{II}}\text{Mn}^{\text{III}}_2\text{Co}^{\text{III}}_2(\text{O})(\text{teaH})_2(\text{dea})(\text{Iso})(\text{OMe})(\text{F})_2(\text{Phen})_2](\text{BF}_4)(\text{NO}_3) \cdot 3\text{MeOH}$  (**6**).

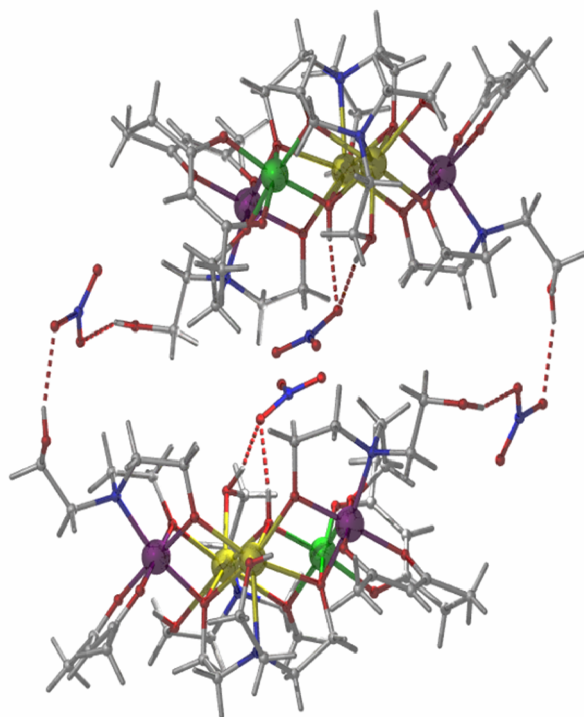


**Fig. S27** Crystal packing for  $[\text{Mn}^{\text{II}}_2\text{Mn}^{\text{III}}\text{Co}^{\text{III}}_2(\text{OH})(\text{teaH})_3(\text{teaH}_2)(\text{acac})_3](\text{NO}_3)_2 \cdot 3\text{CH}_2\text{Cl}_2$  (**7**), showing the pairwise H-bonding cluster formation.